Superradiance in spin-j particles: Effects of multiple levels

G.-D. Lin* and S. F. Yelin
Department of Physics, University of Connecticut, Storrs, Connecticut 06269 and
ITAMP, Harvard-Smithsonian Center for Astrophysics, Cambridge, Massachusetts 02138, USA
(Received 8 December 2011; published 26 March 2012)

We study the superradiance dynamics in a dense system of atoms each of which can be generally a spin-j particle, with j an arbitrary half-integer. We generalize Dicke's superradiance point of view to multiple-level systems and compare the results based on a novel approach we developed previously [Lin and Yelin, Adv. Atom. Mol. Opt. Phys. **61**, in press (2012)]. Using this formalism we derive an effective two-body description that shows cooperative and collective effects for spin-j particles, taking into account the coherence of transitions between different atomic levels. We find that superradiance, which is well known as a many-body phenomenon, can also be modified by multiple-level effects. We also discuss the feasibility and propose that our approach can be applied to polar molecules, for their vibrational states have a multilevel structure which is partially harmonic.

DOI: 10.1103/PhysRevA.85.033831 PACS number(s): 42.50.Nn, 42.50.Ar, 33.20.Tp

I. INTRODUCTION

Quantum many-body physics has been one of the most attractive areas for decades, along with the remarkable advances in the fields of ultracold atomic and molecular systems and quantum optics. These systems not only provide an excellent testbed for study of the quantum nature of various many-body phenomena, such as Bose-Einstein condensation, superfluidity [1–3], quantum magnetism, and quantum phase transitions [4–7], but also inspire the implementation of quantum machinery such as quantum simulation [8–13] and quantum computing [14–16]. In many ways, quantum many-body effects are "exotic" compared to their classical counterparts, and even to quantum single-body physics, mainly due to the particle statistics and indistinguishability of particles. The circumstances can become even more complicated when an ensemble of particles interacts cooperatively, which results in higher-order nonlinear effects. Superradiance, usually representing an N^2 enhancement of the radiation intensity due to coherent decay of a dense sample consisting of N excited atoms, is one important example which can be understood qualitatively through particle indistinguishability and symmetry arguments without the need for considering particle statistics. This phenomenon was first predicted in 1954 by R. H. Dicke [17], who pointed out that the radiative properties of an excited atom can differ greatly just because other atoms are present or not, given that their distance is much smaller than the wavelength of the radiation field even if the particle wave packets do not overlap and no direct interaction is present. Since then, such cooperative effects have been intensively investigated both theoretically and experimentally [18–34]. Recently, superradiance has regained attention for the investigation of the scattering properties of a Bose-Einstein condensate [35–42], alkaline-earth-metal atoms [43], Rydberg atoms [44,45], and quantum dots [46], as well as its strong connections to quantum information through the so-called Dicke states [47–50]. Such states are fully symmetric states by particle permutation and mostly serve as the main stage during the superradiance process.

Traditionally, superradiance deals with two-level atoms or other spin-$\frac{1}{2}$ systems, initially at the excited states, that decay cooperatively. It is natural as the next step to consider particles with larger spins, i.e., systems with a multiple-level structure. Examples include the near-harmonic level structure of low-lying vibrational states in molecules. Generally speaking, a multilevel structure brings up more complications for the radiating system. For example, an excited atom in a higher level is still excited after emitting a photon; atoms and photons from different-level transitions can further cooperate and modify the overall emission behavior. In order to study multilevel effects, we reconsider Dicke's point of view of superradiance as the starting point by first assuming the system to be point-like and fully symmetric.

However, Dicke's picture is only qualitatively correct and is insufficient to describe real situations, where the actual arrangement of particles, the sample's finite size, and dipole-dipole interactions play a role. Microscopically, single atoms build up interatomic coherence due to virtual photon exchange caused by dipole-dipole interaction and form many-body states such as Dicke states [26,51]. The coherence can be breached when the geometry of particle arrangement introduces inhomogeneity such as dipole-dipole interaction between each pair of particles. This leads to dephasing effects and therefore Dicke's picture fails to be valid. To characterize how the "finite size" influences superradiant behavior, a parameter, cooperativity $\mathcal{C} \sim \mathcal{N}\lambda^3$, is introduced, with $\mathcal{N}$ the number density and λ the wavelength of the transition field. One then expects that superradiance is observable for $\mathcal{C} \gg 1$ and is suppressed for small $\mathcal{C}$. Our previous study [45] further suggested the more accurate estimation that the criterion of observing superradiance is approximately given by the optical thickness $\mathcal{N}\lambda^2 l$ (l is the sample size), in agreement with Refs. [19,29,52,53]. To take into account the realistic arrangement of our particle systems, we use a novel formalism that considers only two probe particles, treating the spread of environment atoms in the mean-field approximation, and then take an average over all possible particle pairs [54,55]. This approach enables us to write down an effective master equation, retaining the degrees of freedom of two-body coherence, which can be regarded as a projection of the many-body coherence in the original system.

*guindarl@physics.harvard.edu

This method has been proven to show a good agreement with ongoing experiments with Rydberg atoms [45]. In this paper we further apply this formalism to spin-j systems.

The article is organized as follows: In Sec. II we discuss the original picture proposed by Dicke and generalize the idea to multilevel systems. Section III sketches the formalism developed in Refs. [54,55] and summarizes the governing equations. We then apply this method to multiple levels and present the results in Sec. IV. There we also discuss the differences from the Dicke model and investigate the significance of many-body and multilevel correlations. In Sec. V we further consider the thermal Doppler broadening and calculate the marginal conditions that superradiance can tolerate. Finally, in Sec. VI a dipolar molecular gas is discussed as an example, for which we consider the vibrational states and investigate the superradiance effects from its vibrational states.

II. DICKE SUPERRADIANCE

To gain a qualitative understanding of the Dicke superradiance, we start by considering an ensemble of $(2j+1)$–level atoms confined within a small region, of a size much smaller than the wavelength of the radiation field. In this limit, the particles are indistinguishable viewed by the field and must be regarded as a whole quantum object. To emphasize that the collective radiative behavior is governed solely by many-body effects, we do not assume any instantaneous, i.e., nonradiative, interaction between atoms. The interparticle spacing is large enough that the overlap of particle wave packets is negligible. In other words, the exchange interaction plays no role, nor does the fermionic or bosonic nature of the atoms. Suppose that the transitions are induced by dipoles through the interaction Hamiltonian $V=-\sum_i \vec{p}_i\cdot\vec{E}(\vec{r}_i)$, where $\vec{p}_i$ is the dipole operator of the ith atom and $\vec{E}(\vec{r}_i)$ is the local field at the coordinate $\vec{r}_i$. Under the long-wavelength assumption of the field for a given small system size, the spatial dependence can be eliminated. Therefore $V=-\vec{E}\cdot\sum_i \vec{p}_i=-\sum_{\mu=x,y,z}\wp_\mu(E_\mu^-\hat{D}^-+\text{H.c.})$ in the rotating-wave approximation. Here $\wp_\mu$ is the dipole moment magnitude of an atom in the μ direction, $E_\mu^\pm$ is the positive (negative) frequency component of the field, and $\hat{D}^\pm\equiv\sum_i\sigma_i^\pm$, with $\sigma_i^-\equiv\sum_{m=-J}^{J-1}|m\rangle_i\langle m+1|$ and $\sigma_i^+\equiv(\sigma_i^-)^\dagger$. Note that V does not break the permutation symmetry of the particles. If all the atoms are initially excited, time evolution will only take the state of the system around the fully symmetric manifold, whose eigenstates are usually called the Dicke states (see Fig. 1) [17,51]:

$$|J,M\rangle=\sqrt{\frac{(J+M)!}{(2J)!(J-M)!}}(\hat{J}^-)^{J-M}|J,J\rangle, \tag{1}$$

where $J=Nj$ is the total spin of N spin-j atoms and the integer M denotes the level index that can only go from J through $-J$; the total spin ladder operators $\hat{J}^\pm=\sum_i\hat{j}_i^\pm$ satisfy $\hat{J}^\pm|J,M\rangle=\sqrt{J(J+1)-M(M\pm1)}|J,M\pm1\rangle$, with each $\hat{j}_i^\pm$ satisfying an analogous relation within the ith atom. The emission rate is then given by $W=\sum_M\rho_M W_J(M)$, where ρ_M is the probability of the state being at the Mth level, and the associated collective decay rate is $W_J(M)=\gamma\langle\hat{D}^+\hat{D}^-\rangle_{JM}$, with γ denoting the bare rate in free space.

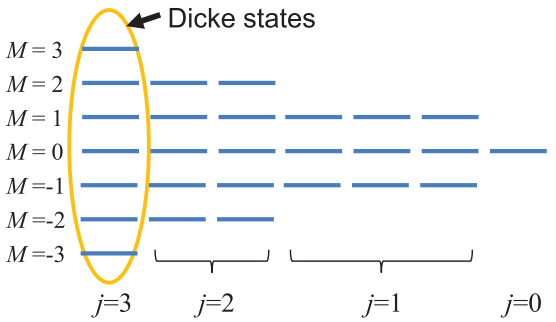

FIG. 1. (Color online) Energy level structure for $N=3$ three-level atoms ($j=1$). There are $(2j+1)^3=27$ levels, including the fully symmetric $2Nj+1=7$ states (Dicke states).

For spin-$\frac{1}{2}$ particles, the ladder operator $\hat{j}_i^\pm$ happens to be, up to a constant factor, equivalent to the dipole transition operator, $\sigma_i^-=|g\rangle_i\langle e|$ and $\sigma_i^+=|e\rangle_i\langle g|$. This connection makes it straightforward to obtain $\langle\hat{D}^+\hat{D}^-\rangle_{JM}=(J+M)(J-M+1)$. For spin-$j>\frac{1}{2}$ atoms, the spin and dipole operators are no longer parallel. To obtain an explicit relation in this case, we take the mean-field assumption and get

$$\begin{aligned}\langle\hat{D}^+\hat{D}^-\rangle_{JM}&=\sum_i\langle\sigma_i^+\sigma_i^-\rangle+\sum_{i\neq j}\langle\sigma_i^+\sigma_j^-\rangle\\&=N\langle\sigma_1^+\sigma_1^-\rangle_{JM}+N(N-1)\langle\sigma_1^+\sigma_2^-\rangle_{JM},\end{aligned} \tag{2}$$

where $\langle\sigma_1^+\sigma_1^-\rangle_{JM}$ and $\langle\sigma_1^+\sigma_2^-\rangle_{JM}$ can be further expressed in terms of the Clebsch-Gordan coefficients, $\langle j_1j_2;m_1m_2|J,M\rangle$:

$$\langle\sigma_1^+\sigma_1^-\rangle=1-\langle j,(N-1)j;-j,M+j|J,M\rangle^2 \tag{3}$$

and

$$\begin{aligned}\langle\sigma_1^+\sigma_2^-\rangle=\sum_{m_1,m_2}[&\langle j,(N-1)j;m_1,M-m_1|J,M\rangle\\&\times\langle j,(N-2)j;m_2,M-m_1-m_2|J-j,M-m_1\rangle\\&\times\langle j,(N-1)j;m_1-1,M-m_1+1|J,M\rangle\\&\times\langle j,(N-2)j;m_2+1,M-m_1-m_2|\\&\times|J-j,M-m_1+1\rangle].\end{aligned} \tag{4}$$

The equation of motion now reads

$$\begin{aligned}\dot{\rho}_{M=J}&=-W_J(J)\rho_J,\\\dot{\rho}_{M<J}&=-W_J(M)\rho_M+W_J(M+1)\rho_{M+1}.\end{aligned} \tag{5}$$

The emission curves of different j's are shown in Fig. 2(b), for which we calculate the intensity per particle $I_{\text{em}}=W(t)/N$, with $N=10$, by evolving Eq. (5). One can observe that every curve shows a different degree of superradiance behavior; i.e., the intensity grows and maximizes in a short period of time. As j increases, the peak intensity becomes higher. This implies that the radiation enhancement comes not only from many-body effects but also from *multiple levels*. This is also shown in Fig. 2(a), where the enhancement factor $\langle\hat{D}^+\hat{D}^-\rangle_{JM}$ as a function of $M-J$ is plotted, consistently explaining the higher emission rate for larger j. One feature worth noting is that all j curves in Fig. 2(b) share the same

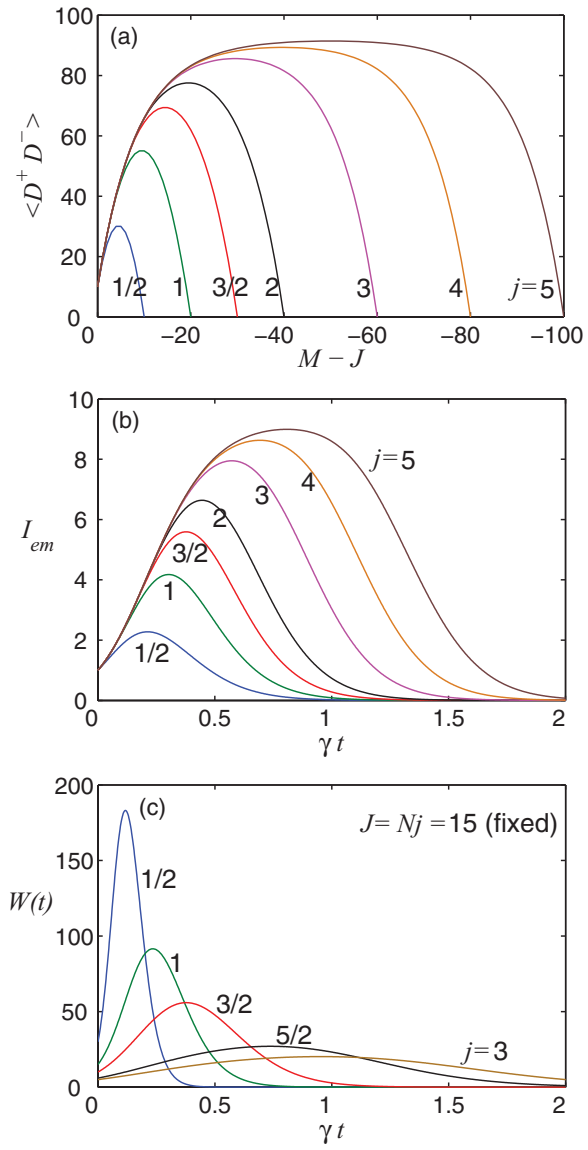

FIG. 2. (Color online) (a) $\langle \hat{D}^+ \hat{D}^- \rangle_{JM}$ as a function of $M - J$; (b) emission intensity per particle $I_{\rm em}$ of different spin j's for $N = 10$ atoms; (c) overall emission curves for different spin j's when $J = Nj = 15$ is fixed. Note that $I_{\rm em}$ and W are in units of $\gamma\hbar\omega_0$, with the energy level spacing $\hbar\omega_0$.

"growing" behavior. This is also suggested by the $\langle \hat{D}^+ \hat{D}^- \rangle_{JM}$ curves in Fig. 2(a): Because we start the radiation process from the fully excited state (the highest collective level), the dynamics is dominantly determined by the population flows associated with a few higher levels. The rates are proportional to the enhancement factor $\langle \hat{D}^+ \hat{D}^- \rangle_{JM}$. For various j, we find in Fig. 2(a) that these curves coincide on the left-hand side, corresponding to $|M - J|$ small (highest levels). Another noticeable feature is that the $\langle \hat{D}^+ \hat{D}^- \rangle_{JM}$ curves develop a plateau as j increases and the highest value is found to be bounded in the large-j limit. It can then be expected that the peak intensity value should also have a bounded value for very large j. We will find that this observation is still true when we use a more sophisticated approach. More details are discussed in Sec. III.

Finally, we compare the overall radiation by different spin-j atoms, keeping the total spin $J = Nj$ fixed. Among these cases, they share the same J-Bloch sphere and therefore might be expected to have similar behaviors. However, this is not true, as we can see from Fig. 2(c). Smaller-j cases have faster and more intense bursts of emission, while larger j's have smoother emission rates and longer tails. This is because $\langle \hat{D}^+ \hat{D}^- \rangle_{JM}$, as determined by Eqs. (3) and (4), is also dependent on N, not merely dependent on the total spin J.

III. EFFECTIVE TWO-BODY FORMALISM

We would like to emphasize that dipole-dipole interaction plays a crucial role and is responsible for both real and virtual photon exchange. As a consequence, the system builds up interparticle coherence while decaying. As dipole-dipole interaction is contained in Dicke's picture, in the sense that the spin flip-flops count, this picture treats the whole system as a point-like object so that the interdipole coupling is considered uniform. In an actual laboratory setup, Dicke's picture is usually an oversimplified view because a real sample always occupies a finite size and sees a finite wavelength of the radiative field. The spatial arrangement of particles usually breaks permutation symmetry. (Or, more precisely, each particle sees different dipole-dipole couplings than all others do.) Nonuniform coupling leads to dephasing of the Dicke states, resulting in population leakage out of the fully symmetric manifold. Furthermore, dipole-dipole interaction also causes other effects, e.g., frequency chirping, for which each Dicke state $|JM\rangle$ can be dipole-dipole shifted differently so that the emission frequency becomes variable over time [24,26,51,56]. Superradiant behavior becomes more complex (and less pronounced) when these effects are not excluded. In order to better describe practical situations, we need to go over the microscopic details of atom-field interactions. The calculation, however, becomes intractable when the number of particles increases typically for $N \gtrsim 10$. In Refs. [45,54,55], we circumvent this difficulty by explicitly writing down the master equation of motion for only two probe atoms, taking the average over the background atoms and tracing out the field variables. We also assume that the field instantaneously interacts with the whole ensemble, ignoring the retardation effects due to the finite size. [This can be justified because the characteristic time of propagation l/c ($\sim 10^{-12}$ s for a sample of size $l \sim 1$ mm) is usually much shorter than any other decay time scales.] We summarize the main results here and leave the details of the derivation to the Appendix. The relevant two-body master equation is given by

$$\dot{\rho} = -\sum_{i,j=1,2} \frac{\Gamma_{ij}}{2}([\rho\sigma_i^-,\sigma_j^\dagger] + [\sigma_i^-,\sigma_j^\dagger\rho]) - \sum_{i,j=1,2} \frac{\Gamma_{ij} + \gamma\delta_{ij}}{2}([\rho\sigma_j^\dagger,\sigma_i^-] + [\sigma_j^\dagger,\sigma_i^-\rho]), \quad (6)$$

where ρ is the two-body density matrix with dimension $(2j+1)^2 \times (2j+1)^2$, $\gamma = \frac{\wp^2\omega_0^3}{3\pi\hbar\epsilon_0 c^3}$ is the free-space spontaneous decay rate, $\Gamma \equiv \Gamma_{ii}$ is the single-particle induced pump/decay rate, and $\bar{\Gamma} \equiv \Gamma_{ij}$ $(i \neq j)$ denotes the two-particle damping rate responsible for the atom-atom correlation. The mean-field

approximation with the second-order correction in fields gives the self-consistent form for the induced rate:

$$\Gamma = \gamma(e^{2\zeta} - 1)\frac{A(t)}{V(t)} + 2\mathcal{C}^2\varrho^4\frac{\gamma^2 I(\zeta,\varrho)}{\Gamma + \gamma/2}Y(t), \tag{7}$$

$$\bar{\Gamma} = \frac{\gamma^2 I(\zeta,\varrho)}{\Gamma + \gamma/2}[3\mathcal{C}\varrho A(t) + 2\mathcal{C}^2\varrho^4 Y(t)], \tag{8}$$

with

$$A(t) = \sum_{m=-j+1}^{j} \rho^{(1)}_{mm}, \tag{9}$$

$$V(t) = \rho^{(1)}_{jj} - \rho^{(1)}_{-j,-j}, \tag{10}$$

$$Y(t) = \sum_{m,m'=-j}^{j-1} \rho_{m+1,m;m',m'+1}, \tag{11}$$

where $\rho^{(1)} \equiv \frac{1}{2}\sum_{i=1,2}\mathrm{tr}_i[\rho]$ denotes the reduced single-particle density matrix and $\rho_{ab;cd} \equiv \frac{1}{2}[\langle a,c|\rho|b,d\rangle + \langle c,a|\rho|d,b\rangle]$. The factor $\frac{1}{2}$ comes from averaging the interchanging of two particles. Note that interchange symmetry requires $\rho_{ab;cd} = \rho_{cd,ab}$ and $\rho^*_{ab;cd} = \rho_{ba;dc}$. The cooperativity parameter is defined as $\mathcal{C} \equiv \mathcal{N}\lambda^3/(4\pi^2)$; $\varrho \equiv \omega l/(2c)$ characterizes the system size l in terms of the radiation wavelength. These results are based on assumptions that there is no external field and hence the generated field has to be on-resonant with the transition frequency. Function $I(\zeta,\varrho) \approx e^{2\zeta}[(\zeta-1)^2 + \varrho^2]/(\zeta^2+\varrho^2)^2$ for large ζ and ϱ. If no thermal broadening is assumed, we have $\zeta \equiv \frac{1}{2}\mathcal{C}\varrho\frac{\gamma}{\Gamma+\gamma/2}V(t)$. When the Doppler broadening needs to be considered, the fields allow detuning, and these quantities must be averaged. More details are discussed in Sec. V.

IV. RESULTS

A. Emission and decay rates

By Eq. (6) we are able to solve for the temporal emission rate curve. Figure 3(a) shows the radiation intensity per particle I_{em} with $\mathcal{C} = 10$ and $\varrho = 10$ for different spin-j species, where $I_{\mathrm{em}} \equiv \hbar\omega_0\sum_{m=-j}^{j}(j+m)\frac{d}{dt}\rho^{(1)}_{mm}(t)$. Here we take $\rho_{jj,jj} = 1$ and set 0 for all other density-matrix elements as the initial state. It can be seen that for each j the radiation intensity reaches a peak, providing strong evidence of superradiance. These curves follow roughly the same intensity profile in the beginning. The maximal value of intensity first grows as j increases from $\frac{1}{2}$ and then stops growing when $j \gtrsim 2$. The time of reaching the peak intensity also converges to a fixed constant $t_{\max}$ in the large-j limit. This has also been observed in the Dicke superradiance picture. Here we give an intuitive explanation as follows: When the system starts to relax from the state with all atoms initially excited to the highest level, only a few highest levels are involved in determining the radiative behavior during the early stage. Even for a very high-spin particle, which has a huge multilevel structure, the levels lower than the first few have not been populated yet and hence do not have contributions. The time evolution of the decay rates is also plotted in Fig. 3(b). Note that at $t = 0$ the diagonal decay rate $\Gamma(0)$ determines the initial emission intensity, followed by sharp growth and, hence, resulting in intensity peaks. In the meantime, the off-diagonal $\bar{\Gamma}$ emerges and mixes single-body states. Differently from the Dicke picture, where we choose the eigenbasis to be the symmetric states constructed by a giant-spin object $J = Nj$, here we use products of single-particle states as the eigenbasis, allowing the degrees of freedom of the population being transferred to asymmetric levels. Note that the dipole-dipole interaction is builtin in our formalism and is responsible for these effects. Consequently, in more realistic cases the superradiance enhancement with j, when characterized by the growth of peak intensity, cannot be as large as predicted by the Dicke model. On the other hand, since the asymmetric levels have lower or vanishing decay rates, the occupation of these levels modifies the tails of the emission curves. In some circumstances, the energy is trapped. Such effects cannot be described by the Dicke model.

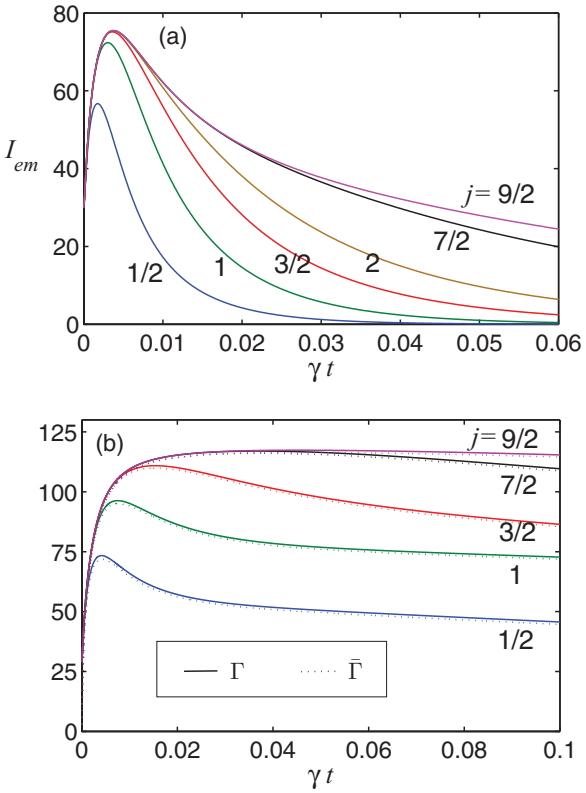

FIG. 3. (Color online) Temporal profiles of (a) the emission intensity per particle (in units of $\gamma\hbar\omega_0$) and (b) the induced single-atom pump/decay rate Γ and two-atom correlation damping rate $\bar{\Gamma}$ (in units of γ). In all cases we use $\mathcal{C} = 10$ and $\varrho = 10$.

A few remarks are made here regarding the connection of cooperativity and superradiant curves. As we increase $\mathcal{C}(\varrho)$ while fixing $\varrho(\mathcal{C})$, the emission peak intensity per particle increases proportionally while the time scale of the initial intensity burst is inversely proportional to $\mathcal{C}(\varrho)$. This is due to "many-body enhancement," as discussed using Dicke's picture. Such features are commonly observed even in the original two-level systems. Further, the emission curves are

found to be similar when $\mathcal{C}\varrho$ is kept the same (not shown). This can also be seen analytically (see the Appendix). This suggests that $\mathcal{C}\varrho \sim \mathcal{N}\lambda^2 l$ is the relevant factor that determines the primary superradiant behavior.

B. Significance of atom-atom coherence

Cooperation of many-body states is crucial to superradiance. The beauty of this formalism is that we retain the accessibility to atom-atom correlations under the framework of the mean-field approximation. Here we investigate the role of many-body correlations, which, in our case, are contained in the off-diagonal terms of the two-body density matrix. To see this, the method allows us to manipulate these off-diagonal terms and evolve Eq. (6). The results are then compared. Note that these off-diagonal terms have the form $\rho_{a,a\pm m;b,b\mp m}$. In the spin-$\frac{1}{2}$ case, the only possibility is $\rho_{eg,ge}(=\rho_{ge,eg})$. Figure 4(a) shows the emission curve for $\mathcal{C} = 10$, $\varrho = 10$, and $\rho_{eg,ge} = 0$ at all times. This curve is now found to be monotonically descending, signaling mere amplified spontaneous emission instead of superradiance because of the apparent lack of an intensity peak. Such monotonicity is shared by larger j cases [Figs. 4(b) and 4(c)] when all off-diagonal terms are set to 0. The reason is clear: Without atom-atom correlation, the density matrix is reduced to a single-particle description and therefore no cooperative effects are observed. On the other hand, for larger j atoms the off-diagonal terms not only concern atom-atom correlations from the same-level transitions but also involve those from different-level density-matrix elements. In the following we try to distinguish the importance of three kinds of coherence terms: (i) same-level coherence $\rho_{a,a\pm1;a\pm1,a}$, (ii) cross-coherence $\rho_{a,a\pm1;b\pm1,b}$ for $a \neq b$, and (iii) higher order coherence $\rho_{a,a\pm m;b,b\mp m}$ for $m \geqslant 2$. For example, in Fig. 4(b) for spin-1 and Fig. 4(c) for spin-$\frac{9}{2}$ atoms, we plot the emission curves corresponding to all off-diagonal terms being dropped out, and (i), (ii), and then (iii) being added back to the system. It is found that with the inclusion of (i) and (ii), the system already behaves like the actual dynamics, indicating that higher order coherence is negligible in determining the evolution of the system. However, if only (i) is included, although intensity enhancement can still be observed, the details of the emission profile show discrepancies from the actual behaviors. The distinction becomes even more obvious when j gets large, as shown in Fig. 4(c). The fact that the cross-coherence terms must be taken into consideration implies that the interferences due to "cross-level" transitions, i.e., degenerate transitions from different levels such as $|a,b \pm 1\rangle \rightarrow |a \pm 1,b\rangle$ with $a \neq b$, make some kind of "multilevel" contributions to the superradiance, analogously to the many-body effects.

V. DOPPLER BROADENING

When a thermal gas is considered, the radiation is inhomogeneously broadened due to the Doppler effect. In this section we consider Doppler broadening when the frequency mismatch causes loss of coherence. Suppose that the thermal

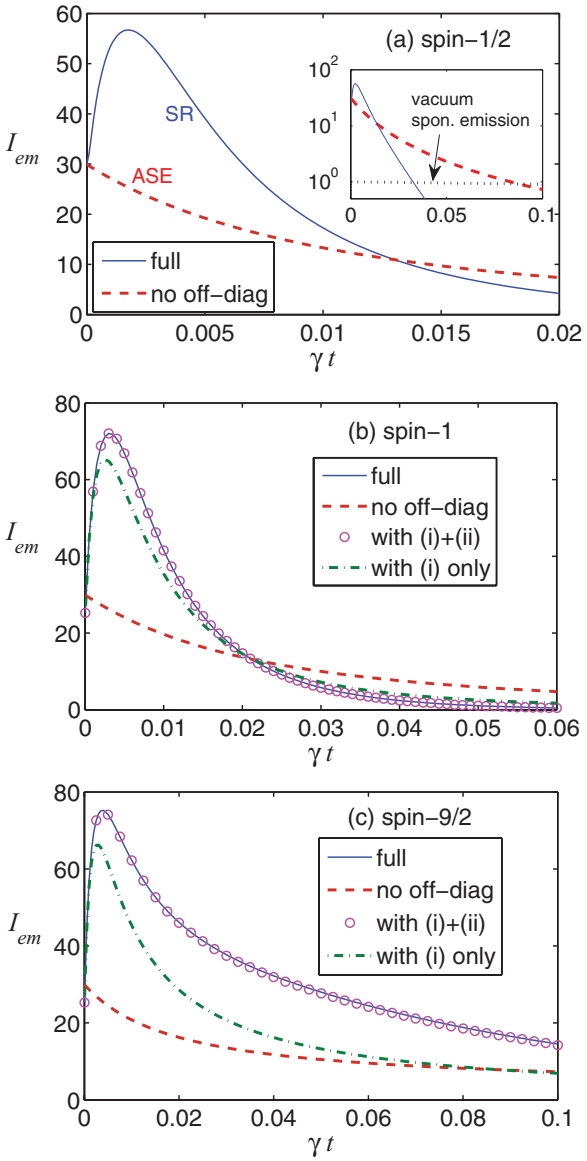

FIG. 4. (Color online) Evolution curves for emission intensity when the off-diagonal terms are fully considered (full), partially removed [with both (i) and (ii) or only with (i); see text], or entirely removed (no off-diag) for (a) spin-$\frac{1}{2}$, (b) spin-1, and (c) spin-$\frac{9}{2}$ particles. Other parameters are the same as in Fig. 3. Inset in (a): Three curves of superradiance [SR; solid (blue) line], amplified spontaneous emission [ASE; dashed (red) line], and single-particle free-space spontaneous emission [dotted (black) line] for comparison.

gas is described by a Gaussian distribution function:

$$f_D(\delta) = \frac{1}{\sqrt{2\pi}\Delta_D} \exp\left[-\frac{\delta^2}{2\Delta_D^2}\right], \tag{12}$$

where δ is the Doppler shift from the transition frequency and $f_D(\delta)d\delta$ is the fraction of the sample within a frequency interval from δ to $\delta + d\delta$ with normalization $\int_{-\infty}^{\infty} f_D(\delta)d\delta = 1$. This distribution is characterized by the Doppler width Δ_D. In order to take the thermal distribution into account, we need to recall the results in Refs. [54,55], also summarized in the Appendix. Consider first the fraction $f_D(\delta)d\delta$ of the

ensemble. The observed field detuning is now $\Delta-\delta$ rather than Δ [cf. Eqs. (A20) and (A21)]. Therefore we can simply calculate the modified rates by replacing Δ with $\Delta'=\Delta-\delta$ in Eqs. (A20) and (A21) because the two integrations deal with only the spatial variables and lead to the same spatial dependence as the nonbroadened case. Special attention must be paid to the source functions, (A22) and (A23), the retarded function, (A25), and Green's function, (A24), which must be treated in an average manner over the distribution f_D because they contain contributions from all fractions. For convenience, we use overbar notation $\bar{Q}=\int_{-\infty}^{\infty}Q(\delta')f_D(\delta')d\delta'$ to represent a Doppler averaged quantity (with the exception of $\bar{\Gamma}$, which denotes the coherence damping rate for consistency). Consequently,

$$\overline{\tilde{P}^{\rm ret}}(\Delta')=\frac{\mathcal{N}\wp^2}{\hbar^2}V(t)\overline{\frac{1}{\Gamma_f-i(\Delta-\delta')}}$$
$$=\frac{\mathcal{N}\wp^2}{\hbar^2}\frac{V(t)}{\Delta_D}\sqrt{\frac{\pi}{2}}U(iz_0), \tag{13}$$

$$\overline{\tilde{P}^{\rm s}}(\Delta')=\frac{\mathcal{N}\wp^2}{\hbar^2}\frac{2A(t)}{\Delta_D}\sqrt{\frac{\pi}{2}}{\rm Re}[U(iz_0)], \tag{14}$$

$$\overline{\tilde{D}^{\rm ret}}(\vec{x},\Delta')=-\frac{i\hbar\omega^2}{6\pi\epsilon_0c^2}\frac{e^{\overline{q_0''}x}}{x}e^{-i\overline{q_0'}x}, \tag{15}$$

where $U(z)\equiv\frac{2}{\sqrt{\pi}}\int_z^\infty e^{z^2-s^2}ds$ is the scaled complementary error function and $z_0=\frac{\Gamma+\gamma/2+i\Delta'}{\sqrt{2}\Delta_D}$; $\overline{q_0''}=\frac{C\gamma\varrho}{d}V(t)\frac{1}{\Delta_D}\sqrt{\frac{\pi}{2}}U(iz_0)$, while $\overline{q_0'}=q_0=\omega/c$ remains the same. Finally, we have

$$\Gamma(\Delta')=\gamma(e^{2\bar{\xi}}-1)\frac{A(t)}{V(t)}$$
$$+2\frac{\gamma^2}{\Delta_D}\mathcal{C}^2\varrho^4I(\bar{\xi},\bar{\varrho}){\rm Re}[U(iz_0)]Y(t), \tag{16}$$

$$\bar{\Gamma}(\Delta')=\frac{\gamma^2}{\Delta_D}I(\bar{\xi},\bar{\varrho}){\rm Re}[U(iz_0)]$$
$$\times[3\mathcal{C}\varrho A(t)+2\mathcal{C}^2\varrho^4Y(t)], \tag{17}$$

where

$$\bar{\varrho}(\Delta')=\varrho+\frac{1}{2}\sqrt{\frac{\pi}{2}}\mathcal{C}\gamma\varrho\frac{V(t)}{\Delta_D}{\rm Re}[U(iz_0)], \tag{18}$$

$$\bar{\xi}(\Delta')=\frac{1}{2}\sqrt{\frac{\pi}{2}}\mathcal{C}\gamma\varrho\frac{V(t)}{\Delta_D}{\rm Im}[U(iz_0)]. \tag{19}$$

In the following we consider only the resonant case by setting $\Delta=0$ because of the absence of an external field. The effective rates are then obtained through averaging over all fractions

$$\Gamma^D=\int_{-\infty}^{\infty}d\delta\frac{1}{\sqrt{2\pi}\Delta_D}e^{-\delta^2/(2\Delta_D^2)}\Gamma(\delta), \tag{20}$$

as well as $\bar{\Gamma}_D$ given in the same manner.

We then calculate the modified emission intensity by solving Eq. (20) numerically, as shown in Fig. 5. With Doppler broadening, it is clear that the superradiance behavior is suppressed as the Doppler width Δ_D increases. This is due to the increase in the frequency mismatch fraction, where the particles lose track of coherence and decay more independently. Note that the extinction of superradiance is a smooth transition rather than an abrupt change. The superradiance peak defers and spreads in time, becoming dimmer in intensity with increasing Δ_D. At very large Δ_D, the peak vanishes and the overall emission curves appear to be monotonically descending. In order to characterize the tolerance that the superradiance can "survive," we define a marginal Doppler width Δ_m beyond which the peak value no longer surpasses the initial intensity, i.e., at $t=0$. Obviously, Δ_m depends on the total number of particles and how these particles are distributed and, hence, the cooperativity parameter $\mathcal{C}$. In Fig. 6 we plot Δ_m as a function of $C\varrho$ for spin-$\frac{1}{2}$ and spin-$\frac{9}{2}$ particles, respectively, with constant $\varrho=10$. It is quite notable that we find approximately a quadratic dependence $\Delta_m\propto\mathcal{C}^2$. This can be understood as follows: As the cooperativity parameter $\mathcal{C}$ is interpreted as the number density, increasing $\mathcal{C}$ not only increases the total number of particles but also makes the sample denser, thus enhancing the dipole-dipole interaction $\wp^2/(2\pi\epsilon_0r^3)\propto r^{-3}\propto\mathcal{C}$. As a result, it is expected that the tolerance Δ_m should be quadratically proportional to $\mathcal{C}$ rather than a linear relation. The "multilevel" enhancement is also observed when comparing Figs. 6(a) and 6(b). This can also be qualitatively understood because, even with fewer particles within the frequency matching zone when the distribution

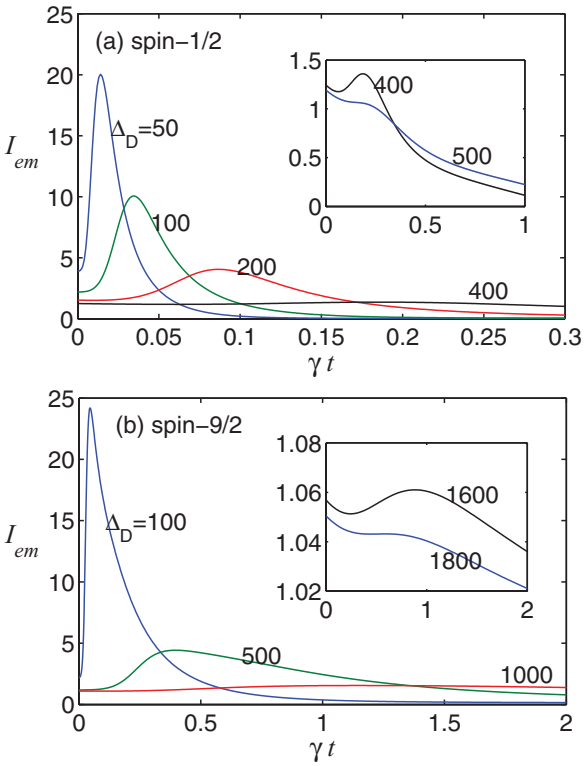

FIG. 5. (Color online) Doppler-broadened emission intensity curves for (a) spin-$\frac{1}{2}$ and (b) spin-$\frac{9}{2}$ particles at various characteristic Doppler widths Δ_D. Here we use $\mathcal{C}=10$ and $\varrho=10$ for both cases. Insets: For each spin particle, we plot two curves, corresponding to Δ_D slightly smaller and slightly larger than the marginal Doppler width Δ_m. Explicitly, in (a) we plot $\Delta_D/\gamma=400$ and 500 for $\Delta_m/\gamma=433$; in (b), $\Delta_D/\gamma=1700$ and 1800 for $\Delta_m/\gamma=1650$.

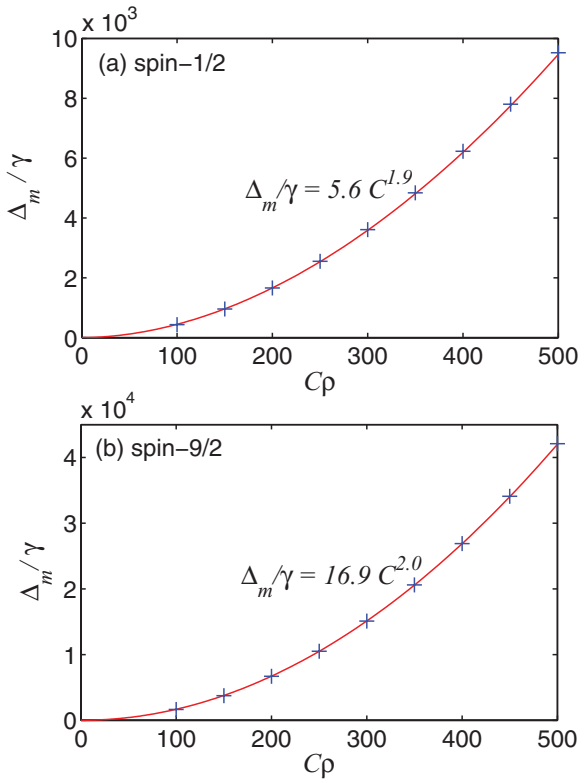

FIG. 6. (Color online) Marginal Doppler width Δ_m as a function of the cooperativity for (a) spin-$\frac{1}{2}$ and (b) spin-$\frac{9}{2}$ particles. Here we take $\varrho = 10$. Crosses (blue) represent our calculated data; solid (red) lines are the best-fitting power-law curves with an exponent close to 2.

is broad, more near-resonant transitions are still allowed for particles with more levels.

VI. MOLECULAR VIBRATIONAL STATES

One direct example of multilevel structure is vibrational modes of polar molecules, where the deeply bound potential can be well approximated by a harmonic one. The number of low-lying eigenstates that are quasi–equally spaced energy levels is usually up to a few tens. These particles are thus analogous to high-"spin" particles. Take the typical example of heteronuclear diatomic alkali molecules [57]: the state $X\,^1\Sigma^+$ for LiCs has an averaged energy spacing $\omega_0 \approx 2\pi \times 5$ THz. For a sample of LiCs molecules with a density $\mathcal{N} \approx 4 \times 10^9$ cm^{-3}, this energy spacing corresponds to cooperativity $\mathcal{C} \sim 20 \gg 1$. The transitional dipole moment between two adjacent vibrational states is about 5 D, and therefore the single-particle spontaneous emission rate $\gamma \sim \mathrm{s}^{-1}$. We then expect, within this parameter regime, that the superradiance intensity peak can be observed on a time scale of milliseconds while $\Gamma_{\max} \gtrsim 1000\gamma$.

The cascade relaxation of an excited population from higher to lower levels is reminiscent of motional cooling. When the cooperative effect comes into play, the down-ladder process will be accelerated because the stimulated decay becomes dominant while superradiance takes place (without other pumping processes such as thermal excitation). As we have pointed out, the induced rate can be a few orders of magnitude upon increasing the number of particles and hence the cooperativity. This suggests a scheme of "superradiance-assisted cooling." This scheme may be an alternative to cool vibrational states of molecules, which, generally speaking, have previously been obstructed by the fact that such states are only weakly optically coupled.

VII. CONCLUSION

We have investigated the superradiance cascade for a dense ensemble of multilevel, or spin-j, particles. Our main results are summarized as follows: (1) While superradiance is known as many-body enhanced radiation in an ensemble, the decay process can be further facilitated by the presence of multiple levels. This multilevel enhancement is due to cooperative emission by correlating different levels. (2) Such multilevel effects get stronger as the quantum number j increases but saturate when j becomes too large. This is because only populations in higher levels come into play within the time scale of the buildup of particle coherence and, meanwhile, superradiation. Both of these features can be seen in the ideal generalized Dicke model and our effective two-body mean-field description. The former method provides generally a more pedagogical picture of superradiance, neglecting the finite-size effect and dephasing due to inhomogeneous dipole interaction, while these nonideal but more realistic factors are considered in the latter approach. (3) Our approach further suggests a way to differentiate the importance of different types of coherence. We find that although interparticle coherence is essential to superradiance, the higher-order off-diagonal terms (involving nonadjacent level transitions) play a negligible role. In addition, cooperation between "cross levels" is evident. (4) We also study the fade-out of superradiance, as a consequence of the fact that the frequency mismatch part of the gas gradually takes over the near-resonance part when a thermal distribution is introduced. By calculating the tolerance of superradiance in terms of the thermal width, we show that the particle density, which determines the strength of dipole-dipole interaction, is an important parameter, as is the total number. (5) We, finally, assess the feasibility of applying our results to dipolar molecular systems, where the transitions between harmonic ladders of vibrational states are to be considered. Our estimation of the relevant laboratory parameters suggests that the results predicted in this paper should be observable using the current experimental technology.

ACKNOWLEDGMENTS

The authors wish to thank Marc Repp, Juris Ulmanis, Johannes Deiglmayr, and Matthias Weidemüller for helpful input. We thank the NSF for financial support.

APPENDIX: EFFECTIVE TWO-BODY MASTER EQUATION

Although this method for effective two-body description has been discussed in great detail in Refs. [54,55], we summarize here the derivation of the formalism, for completeness.

We start with the microscopic Hamiltonian, which reads

$$H = \underbrace{H_{\text{atom}} + H_{\text{field}} - \sum_{j\notin\{1,2\}} \vec{p}_j \cdot [\vec{\mathcal{E}}(\vec{r}_i,t) + \vec{E}(\vec{r}_j,t)]}_{H_0} - \underbrace{\sum_{i=1}^{2} \vec{p}_i \cdot [\vec{\mathcal{E}}(\vec{r}_i,t) + \vec{E}(\vec{r}_i,t)]}_{V}. \tag{A1}$$

Here, we separate the field into two parts: the external classical driving field $\vec{\mathcal{E}}(\vec{r}_i,t)$ and the induced local field $\vec{E}(\vec{r}_i,t)$. When a uniform dense gas of atoms is considered, it is reasonable to assume that every atom sees the same field and the same background due to other atoms. On the other hand, in order to take into account atom-atom quantum correlation, we need to retain adequate degrees of freedom involving at least two particles. Our proposal is therefore to write an effective description for two probe atoms such that all other atoms' contribution will be averaged in the mean-field sense. In Eq. (A1) V is the field-atom interaction only of the probe atoms ($i = 1, 2$) and is treated as a small perturbation. H_0 consists of the unperturbed atomic and field Hamiltonian as well as the contribution from the background atoms. In the interaction picture, the evolution operator is given by

$$S_I(t) = T \exp\left[-\frac{i}{\hbar}\int_{-\infty}^{t} V_I(t')dt'\right], \tag{A2}$$

where T is the time-ordering operator. We here introduce the positive and negative components $x(t) = x^+(t) + x^-(t)$ with $x^\pm(t) = \widetilde{x}(t)e^{\mp i\omega t}$, where $x \in \{p_{i\mu}, E_\mu, \mathcal{E}_\mu\}$ with $\mu = x$, y, z and the amplitude $\widetilde{x}(t)$ is slowly varying compared to the inverse of the radiation frequency ω^{-1}. The polarization operator is related to the transition operator through $\widetilde{p}^+_{i\mu} = \wp_\mu \sigma_i^-$ and $\widetilde{p}^-_{i\mu} = \wp_\mu \sigma_i^+$, with the magnitude $\wp_\mu$ assumed to be real. In the rotating-wave approximation, the interaction becomes $V_I(t) \simeq \sum_{i\mu}[p^+_{i\mu}(E^-_\mu + \mathcal{E}^-_\mu) + \text{H.c.}]$. Equation (A2) can be cast in the framework of the Schwinger-Keldysh formalism, in which $V_I(t) \longrightarrow V(\check{\tau})$ and $S_I(t) \longrightarrow$

$$S_C = T_C \exp\left[-\frac{i}{\hbar}\int_C V(\check{\tau})d\check{\tau}\right], \tag{A3}$$

where C denotes the Schwinger-Keldysh contour as shown in Fig. 7, and T_C is the contour-oriented time-ordering operator; i.e., along the upper branch of the contour T_C is the normal time-ordering operator, while along the lower branch it is the inverse time-ordering operator. To prevent possible confusion we denote the contour-oriented "time" parameter as $\check{\tau}$ (with a haček). We then trace out the degrees of freedom of the fields and the background atoms, which leads to an effective evolution operator,

$$S_C^{\text{eff}} = \langle S_C\rangle_{\text{field}} = T_C \exp\left\{\frac{i}{\hbar}\int_C d\check{\tau}\sum_{i=1}^{2}\sum_{\mu}[p^+_{i\mu}(\check{\tau})\mathcal{E}^-_{L\mu}(\vec{r}_i,\check{\tau}) + p^-_{i\mu}(\check{\tau})\mathcal{E}^+_{L\mu}(\vec{r}_i,\check{\tau})] - \frac{1}{2\hbar^2}\int\int_C d\check{\tau}_1 d\check{\tau}_2 \sum_{i,j=1}^{2}\sum_{\mu\nu} \times [p^+_{i\mu}(\check{\tau}_1)D_{i\mu,j\nu}(\check{\tau}_1,\check{\tau}_2)p^-_{j\nu}(\check{\tau}_2) + p^-_{i\mu}(\check{\tau}_1)C_{i\mu,j\nu}(\check{\tau}_1,\check{\tau}_2)p^+_{j\nu}(\check{\tau}_2)]\right\}, \tag{A4}$$

where $\vec{\mathcal{E}}^\pm_L(\vec{r}_i,\check{\tau}) = \vec{\mathcal{E}}^\pm(\vec{r}_i,\check{\tau}) + \langle\vec{E}^\pm(\vec{r}_i,\check{\tau})\rangle$ is the local field seen by the probe atom i, and the Green's function of the interacting field,

$$D_{i\mu,j\nu}(\check{\tau}_1,\check{\tau}_2) = \langle\langle T_C E^-_\mu(\vec{r}_i,\check{\tau}_1)E^+_\nu(\vec{r}_j,\check{\tau}_2)\rangle\rangle \tag{A5}$$

$$C_{i\mu,j\nu}(\check{\tau}_1,\check{\tau}_2) = \langle\langle T_C E^+_\mu(\vec{r}_i,\check{\tau}_1)E^-_\nu(\vec{r}_j,\check{\tau}_2)\rangle\rangle. \tag{A6}$$

To obtain Eq. (A4) we used

$$\langle T_C \exp[s\hat{A}]\rangle = \exp\left[\sum_m \frac{s^m}{m!}\langle\langle T_C \hat{A}^m\rangle\rangle\right], \tag{A7}$$

with $\langle\langle\cdot\rangle\rangle$ denoting the cumulant, defined by

$$\langle\langle\hat{A}\rangle\rangle = \langle\hat{A}\rangle, \quad \langle\langle\hat{A}\hat{B}\rangle\rangle = \langle\hat{A}\hat{B}\rangle - \langle\hat{A}\rangle\langle\hat{B}\rangle,$$

where $\hat{A}$ and $\hat{B}$ are operators. We also set the higher order cumulants $\langle\langle E^m\rangle\rangle = 0$ for $m > 2$ by assuming that the radiation field is Gaussian. The two-field Green's function $D_{i\mu,j\nu}(\check{\tau}_1,\check{\tau}_2)$, depending on the order of $\check{\tau}_1$ and $\check{\tau}_2$ on C, has four possible forms:

$$D^{++}_{i\mu,j\nu} = \langle\langle T E^-_\mu(\vec{r}_i,\tau_{1+})E^+_\nu(\vec{r}_j,\tau_{2+})\rangle\rangle, \tag{A8}$$

$$D^{--}_{i\mu,j\nu} = \langle\langle T^{-1} E^-_\mu(\vec{r}_i,\tau_{1-})E^+_\nu(\vec{r}_j,\tau_{2-})\rangle\rangle, \tag{A9}$$

$$D^{-+}_{i\mu,j\nu} = \langle\langle E^-_\mu(\vec{r}_i,\tau_{1-})E^+_\nu(\vec{r}_j,\tau_{2+})\rangle\rangle, \tag{A10}$$

$$D^{+-}_{i\mu,j\nu} = \langle\langle E^+_\nu(\vec{r}_j,\tau_{2-})E^-_\mu(\vec{r}_i,\tau_{1+})\rangle\rangle. \tag{A11}$$

Here we have added the subscript $+$ or $-$ to τ (but no haček, meaning that it is now a "regular" time variable) to keep track of its original location, i.e., the upper or lower branch, respectively, on the Schwinger-Keldysh contour C. The other Green's function $C_{i\mu,j\nu}$ has analogous forms. We then rewrite the double-integral involving $D_{i\mu,j\nu}$ in Eq. (A4) as

$$\int\int_C d\check{\tau}_1 d\check{\tau}_2 p^+_{i\mu}(\check{\tau}_1)D_{i\mu,j\nu}(\check{\tau}_1,\check{\tau}_2)p^-_{j\nu}(\check{\tau}_2) = \sum_{A,B\in\{+,-\}}\kappa_{AB}\wp_\mu\wp_\nu\int_{-\infty}^{\infty}d\tau_1\int_{-\infty}^{\infty}d\tau_2 \times \sigma^-_{iA}D^{AB}_{i\mu,j\nu}(\tau_1,\tau_2)\sigma^+_{jB}e^{i\omega(\tau_2-\tau_1)}, \tag{A12}$$

where $\kappa_{AB} = 1$ for $A = B$ and $\kappa_{AB} = -1$ for $A \neq B$. Again, we have added the subscripts A and B ($A, B \in \{+,-\}$) to σ^- and σ^+ to remind us of their order on the Schwinger-Keldysh

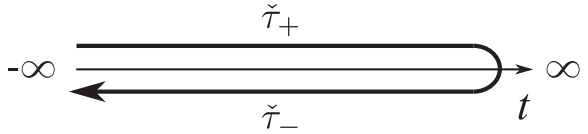

FIG. 7. Schwinger-Keldysh contour.

contour C. After some math, we reach

$$\begin{aligned} S_C^{\rm eff} = T_c \exp\Bigg\{ & \sum_{i,\mu} \frac{i\wp_\mu}{\hbar} \int_{-\infty}^{\infty} d\tau [\sigma_{i+}^- \mathcal{E}_{L\mu}^-(\vec{r}_i,\tau) \\ & - \sigma_{i-}^- \mathcal{E}_{L\mu}^-(\vec{r}_i,\tau) + \sigma_{i+}^+ \mathcal{E}_{L\mu}^+(\vec{r}_i,\tau) - \sigma_{i-}^+ \mathcal{E}_{L\mu}^+(\vec{r}_i,\tau)] \\ & - \int_{-\infty}^{\infty} d\tau \frac{\Gamma_{i\mu,jv}}{2} [\sigma_{i+}^- \sigma_{j+}^+ + \sigma_{i-}^- \sigma_{j-}^+ - 2\sigma_{i-}^- \sigma_{j+}^+] \\ & - \int_{-\infty}^{\infty} d\tau \frac{\Gamma_{i\mu,jv} + \gamma_{i\mu,jv}}{2} [\sigma_{j+}^+ \sigma_{i+}^- + \sigma_{j-}^+ \sigma_{i-}^- \\ & - 2\sigma_{j-}^+ \sigma_{i+}^-] + \frac{i}{\hbar} \int_{-\infty}^{\infty} d\tau H_{i\mu,jv} [\sigma_{i+}^- \sigma_{j+}^+ \\ & - \sigma_{i-}^- \sigma_{j-}^+ - \sigma_{j+}^+ \sigma_{i+}^- + \sigma_{j-}^+ \sigma_{i-}^-] \\ & + \frac{i}{\hbar} \int_{-\infty}^{\infty} d\tau h_{i\mu,jv} [\sigma_{j+}^+ \sigma_{i+}^- + \sigma_{j-}^+ \sigma_{i-}^-] \Bigg\}. \end{aligned} \tag{A13}$$

Here we introduce

$$\begin{aligned} \Gamma_{i\mu,jv}(\tau;\Delta) = & \frac{\wp_\mu \wp_v}{\hbar^2} \int_{-\infty}^{\infty} d\tau' \langle\langle E_\mu^-(\vec{r}_i,\tau) \\ & \times E_v^+(\vec{r}_j,\tau+\tau')\rangle\rangle e^{i\omega\tau'}, \end{aligned} \tag{A14}$$

$$\begin{aligned} \gamma_{i\mu,jv}(\tau;\Delta) = & \frac{\wp_\mu \wp_v}{\hbar^2} \int_{-\infty}^{\infty} d\tau' \langle [E_\mu^+(\vec{r}_i,\tau), \\ & E_v^-(\vec{r}_j,\tau+\tau')]\rangle e^{i\omega\tau'}, \end{aligned} \tag{A15}$$

$$\begin{aligned} H_{i\mu,jv}(\tau;\Delta) = & \frac{i\wp_\mu \wp_v}{2\hbar} \int_0^{\infty} d\tau' \{\langle\langle E_\mu^-(\vec{r}_i,\tau) E_v^+(\vec{r}_j,\tau-\tau')\rangle\rangle \\ & \times e^{-i\omega\tau'} - \langle\langle E_\mu^-(\vec{r}_i,\tau) E_v^+(\vec{r}_j,\tau+\tau')\rangle\rangle e^{i\omega\tau'}\}, \end{aligned} \tag{A16}$$

$$\begin{aligned} h_{i\mu,jv}(\tau;\Delta) = & \frac{i\wp_\mu \wp_v}{2\hbar} \int_0^{\infty} d\tau' \{\langle [E_\mu^-(\vec{r}_i,\tau), E_v^+(\vec{r}_j,\tau-\tau')]\rangle \\ & \times e^{-i\omega\tau'} - \langle [E_\mu^-(\vec{r}_i,\tau), E_v^+(\vec{r}_j,\tau+\tau')]\rangle e^{i\omega\tau'}\}, \end{aligned} \tag{A17}$$

where we have changed the time variables such that $D_{i\mu,jv}^{AB}(\tau_1,\tau_2) \longrightarrow D_{i\mu,jv}^{AB}(\tau,\tau')$, with $\tau_1 = \tau - \tau'/2$ and $\tau_2 = \tau + \tau'/2$. The right-hand side of Eqs. (A14)–(A17) is reminiscent of the Fourier transformation with respect to the time distance τ'. $\Delta = \omega - \omega_0$ is the frequency detuning of the field from the atomic spacing ω_0. Without the presence of an external field, the radiation mainly comes from atomic transitions, so that $\Delta = 0$ for such resonant cases. But here we first keep Δ explicitly, for generality.

From Eq. (A13) we extract the effective master equation:

$$\begin{aligned} \dot{\rho}(t) = & -\frac{i}{\hbar}[H_0,\rho] \\ & + \sum_{j=1,2} \sum_{\mu} \frac{i}{\hbar} \wp_\mu [\sigma_j^- \mathcal{E}_{L,\mu}^-(\vec{r}_j) + \sigma_j^\dagger \mathcal{E}_{L,\mu}^+(\vec{r}_j), \rho] \\ & + \frac{i}{\hbar} \sum_{i=1,2} \sum_{\mu,v} H_{i\mu,iv}(t) [[\sigma_{i\mu}^-, \sigma_{iv}^+], \rho] \\ & - \sum_{i,j=1,2} \sum_{\mu,v} \frac{\Gamma_{i\mu,jv}(t)}{2} ([\rho\sigma_i^-, \sigma_j^\dagger] + [\sigma_i^-, \sigma_j^\dagger \rho]) \\ & - \sum_{i,j=1,2} \sum_{\mu,v} \frac{\Gamma_{i\mu,jv}(t) + \gamma_{i\mu,jv}(t)}{2} \\ & \times ([\rho\sigma_j^\dagger, \sigma_i^-] + [\sigma_j^\dagger, \sigma_i^- \rho]). \end{aligned} \tag{A18}$$

Note that the two-body density operator ρ is a $(2j+1)^2 \times (2j+1)^2$ matrix. We can now identify term Γ as the induced pump/decay rate and term γ as the spontaneous decay rate inside the atomic medium. Term h as shown in Eq. (A17) corresponds to the Lamb shifts, which are somewhat irrelevant for our current consideration, and is therefore absorbed by the unperturbed Hamiltonian H_0; term H as shown in Eq. (A16) accounts for the collective light shifts and inhomogeneous broadening. In this paper, we neglect dipole shifts and frequency chirping by dropping the term H and focus strictly on the quantum correction relevant to superradiance. To slightly ease the computational complication, we directly take γ as the free-space rate (see Appendix A in Ref. [55]) and consider only a single polarization component of the field so that subscripts μ and v can also be dropped. The relevant part of the master equation now reads

$$\begin{aligned} \dot{\rho} = & -\sum_{i,j=1,2} \frac{\Gamma_{ij}}{2} ([\rho\sigma_i^-, \sigma_j^\dagger] + [\sigma_i^-, \sigma_j^\dagger \rho]) \\ & - \sum_{i,j=1,2} \frac{\Gamma_{ij} + \gamma\delta_{ij}}{2} ([\rho\sigma_j^\dagger, \sigma_i^-] + [\sigma_j^\dagger, \sigma_i^- \rho]). \end{aligned} \tag{A19}$$

By following the derivation in Refs. [54,55] we are able to calculate the right-hand side of Eq. (A14) through

$$\begin{aligned} \Gamma(t;\Delta) = & \frac{\wp^2}{\hbar^2} \int d^3x |\widetilde{D}^{\rm ret}(t;\vec{x},\Delta)|^2 \widetilde{P}^{(1)\rm s}(t;\Delta) \\ & + \frac{\wp^2}{\hbar^2} \int\int d^3x_1 d^3x_2 \widetilde{D}^{\rm ret}(t;\vec{x}_1,\Delta) \\ & \times \widetilde{D}^{*\rm ret}(t;\vec{x}_2,\Delta) \widetilde{P}^{(2)\rm s}(t;\Delta), \end{aligned} \tag{A20}$$

$$\begin{aligned} \bar{\Gamma}(t;\Delta) = & \frac{\wp^2}{\hbar^2} \int d^3x \widetilde{D}^{\rm ret}(t;\vec{x},\Delta) \widetilde{D}^{*\rm ret}(t;\vec{x},\Delta) \widetilde{P}^{(1)\rm s}(t;\Delta) \\ & + \frac{\wp^2}{\hbar^2} \int\int d^3x_1 d^3x_2 \widetilde{D}^{\rm ret}(t;\vec{x}_1,\Delta) \\ & \times \widetilde{D}^{*\rm ret}(t;\vec{x}_2,\Delta) \widetilde{P}^{(2)\rm s}(t;\Delta). \end{aligned} \tag{A21}$$

We now denote $\Gamma \equiv \Gamma_{ii}$ and $\bar{\Gamma} \equiv \Gamma_{ij}$ for $i \neq j$. We have also replaced $\vec{r}_i$ and $\vec{r}_j$ with $\vec{r}_0 = (\vec{r}_i + \vec{r}_j)/2$ and $\vec{x} = \vec{r}_i - \vec{r}_j$. But $\vec{r}_0$ dependence is then dropped because of the assumption of a small sample. The single-particle source function $\widetilde{P}^{(1)\rm s}$ and the two-particle one $\widetilde{P}^{(2)\rm s}$ are given, respectively, by

$$\widetilde{P}^{(1)\rm s}(t;\Delta) = \frac{\mathcal{N}\wp^2}{\hbar^2} \left[\frac{2A(t)\left(\frac{\gamma}{2}+\Gamma\right)}{\left(\frac{\gamma}{2}+\Gamma\right)^2 + \Delta^2} \right], \tag{A22}$$

$$\widetilde{P}^{(2)\rm s}(t;\Delta) = \frac{\mathcal{N}^2\wp^2}{\hbar^2} \left[\frac{2Y(t)\left(\frac{\gamma}{2}+\Gamma\right)}{\left(\frac{\gamma}{2}+\Gamma\right)^2 + \Delta^2} \right], \tag{A23}$$

with $\mathcal{N}$ the particle volume density. Quantities $A(t)$, $V(t)$, and $Y(t)$ are determined by the density matrix through

Eqs. (9)–(11). In addition, the retarded Green's function is

$$\widetilde{D}^{\rm ret}(t;\vec{x},\Delta) = -\frac{i\hbar\omega^2}{6\pi\epsilon_0 c^2}\frac{e^{q_0'' x}}{x}e^{-iq_0' x}, \tag{A24}$$

with $q_0' = \omega/c$ and $q_0'' = \frac{\hbar\omega}{3\epsilon_0 c}\widetilde{P}^{\rm ret}(t;\Delta)$, where the retarded function

$$\widetilde{P}^{\rm ret}(t;\Delta) = \frac{\mathcal{N}\wp^2}{\hbar^2}\left[\frac{V(t)}{\left(\frac{\gamma}{2}+\Gamma\right)-i\Delta}\right]. \tag{A25}$$

Through direct integration we finally get

$$\Gamma = \gamma(e^{2\zeta}-1)\frac{A(t)}{V(t)} + 2\mathcal{C}^2\varrho^4\frac{\gamma^2 I(\zeta,\tilde{\varrho})}{\Gamma+\gamma/2}Y(t), \tag{A26}$$

$$\bar{\Gamma} = \frac{\gamma^2 I(\zeta,\tilde{\varrho})}{\Gamma+\gamma/2}[3\mathcal{C}\varrho A(t) + 2\mathcal{C}^2\varrho^4 Y(t)], \tag{A27}$$

with

$$\mathcal{C} = \mathcal{N}\lambda^3/(4\pi^2), \quad \varrho = \pi l/\lambda,$$
$$\zeta = \frac{1}{2}\mathcal{C}\varrho\frac{\gamma(\Gamma+\gamma/2)}{(\Gamma+\gamma/2)^2+\Delta^2}V(t),$$
$$\tilde{\varrho} = \varrho - \Delta\zeta/(\Gamma+\gamma/2),$$
$$I(\zeta,\rho) = e^{2\zeta}[(\zeta-1)^2+\varrho^2]/(\zeta^2+\varrho^2)^2.$$

It is worth noting that in Eq. (A26), $\zeta = \zeta(\mathcal{C}\varrho)$, and the second term is proportional to $\mathcal{C}^2\varrho^4 e^{2\zeta}/(\zeta^2+\varrho^2) \sim \mathcal{C}^2\varrho^2 e^{2\zeta}$ for $\varrho \gg \zeta$ and is usually insensitive when varying $\mathcal{C}$ and ϱ separately. As a result, the product $\mathcal{C}\varrho$ turns out to be a determinant factor for superradiance dynamics even though the individual dependence on $\mathcal{C}$ and ϱ is still evident, but less significant, in most cases.

[1] M. H. Anderson, J. R. Ensher, M. R. Matthews, C. E. Wieman, and E. A. Cornell, Science **269**, 198 (1995).
[2] M. Greiner, C. A. Regal, and D. S. Jin, Nature **426**, 537 (2003).
[3] A. J. Leggett, Rev. Mod. Phys. **73**, 307 (2001).
[4] M. P. A. Fisher, P. B. Weichman, G. Grinstein, and D. S. Fisher, Phys. Rev. B **40**, 546 (1989).
[5] M. Greiner, O. Mandel, T. Esslinger, T. W. Hansch, and I. Bloch, Nature **415**, 39 (2002).
[6] Z. Hadzibabic, P. Kruger, M. Cheneau, B. Battelier, and J. Dalibard, Nature **441**, 1118 (2006).
[7] H. Weimer, R. Löw, T. Pfau, and H. P. Büchler, Phys. Rev. Lett. **101**, 250601 (2008).
[8] L.-M. Duan, E. Demler, and M. D. Lukin, Phys. Rev. Lett. **91**, 090402 (2003).
[9] D. Porras and J. I. Cirac, Phys. Rev. Lett. **92**, 207901 (2004).
[10] A. Friedenauer, H. Schmitz, J. T. Glueckert, D. Porras, and T. Schaetz, Nat. Phys. **4**, 757 (2008).
[11] R. Gerritsma, G. Kirchmair, F. Zahringer, E. Solano, R. Blatt, and C. F. Roos, Nature **463**, 68 (2010).
[12] K. Kim, M.-S. Chang, S. Korenblit, R. Islam, E. E. Edwards, J. K. Freericks, G.-D. Lin, L.-M. Duan, and C. Monroe, Nature **465**, 590 (2010).
[13] Y.-J. Lin, R. L. Compton, K. Jimenez-Garcia, J. V. Porto, and I. B. Spielman, Nature **462**, 628 (2009).
[14] G. K. Brennen, C. M. Caves, P. S. Jessen, and I. H. Deutsch, Phys. Rev. Lett. **82**, 1060 (1999).
[15] E. Kuznetsova, T. Bragdon, R. Côté, and S. F. Yelin, Phys. Rev. A **85**, 012328 (2012).
[16] E. Kuznetsova, S. T. Rittenhouse, H. R. Sadeghpour, and S. F. Yelin, Phys. Chem. Chem. Phys. **13**, 17115 (2011).
[17] R. H. Dicke, Phys. Rev. **93**, 99 (1954).
[18] G. Feher, J. P. Gordon, E. Buehler, E. A. Gere, and C. D. Thurmond, Phys. Rev. **109**, 221 (1958).
[19] F. T. Arecchi and E. Courtens, Phys. Rev. A **2**, 1730 (1970).
[20] R. H. Lehmberg, Phys. Rev. A **2**, 883 (1970).
[21] N. E. Rehler and J. H. Eberly, Phys. Rev. A **3**, 1735 (1971).
[22] R. Bonifacio, P. Schwendimann, and F. Haake, Phys. Rev. A **4**, 302 (1971).
[23] R. Friedberg and S. Hartmann, Phys. Lett. A **37**, 285 (1971).
[24] C. R. Stroud, J. H. Eberly, W. L. Lama, and L. Mandel, Phys. Rev. A **5**, 1094 (1972).
[25] N. Skribanowitz, I. P. Herman, J. C. MacGillivray, and M. S. Feld, Phys. Rev. Lett. **30**, 309 (1973).
[26] F. De Martini and G. Preparata, Phys. Lett. A **48**, 43 (1974).
[27] R. Jodoin and L. Mandel, Phys. Rev. A **9**, 873 (1974).
[28] R. Bonifacio and L. A. Lugiato, Phys. Rev. A **11**, 1507 (1975).
[29] J. C. MacGillivray and M. S. Feld, Phys. Rev. A **14**, 1169 (1976).
[30] F. Gounand, M. Hugon, P. R. Fournier, and J. Berlande, J. Phys. B **12**, 547 (1979).
[31] R. Prakash and N. Chandra, Phys. Rev. A **21**, 1297 (1980).
[32] P. Goy, J. M. Raimond, M. Gross, and S. Haroche, Phys. Rev. Lett. **50**, 1903 (1983).
[33] L. Moi, P. Goy, M. Gross, J. M. Raimond, C. Fabre, and S. Haroche, Phys. Rev. A **27**, 2043 (1983).
[34] A. Crubellier, J. Phys. B **20**, 971 (1987).
[35] M. G. Moore and P. Meystre, Phys. Rev. Lett. **83**, 5202 (1999).
[36] S. Inouye, A. P. Chikkatur, D. M. Stamper-Kurn, J. Stenger, D. E. Pritchard, and W. Ketterle, Science **285**, 571 (1999).
[37] O. E. Müstecaplioğlu and L. You, Phys. Rev. A **62**, 063615 (2000).
[38] W. Ketterle, A. P. Chikkatur, and C. Raman, AIP Conf. Proc. **551**, 337 (2001).
[39] N. Piovella, R. Bonifacio, B. W. J. McNeil, and G. R. M. Robb, Opt. Commun. **187**, 165 (2001).
[40] M. M. Cola and N. Piovella, Phys. Rev. A **70**, 045601 (2004).
[41] K. Baumann, C. Guerlin, F. Brennecke, and T. Esslinger, Nature **464**, 1301 (2010).
[42] D. Nagy, G. Kónya, G. Szirmai, and P. Domokos, Phys. Rev. Lett. **104**, 130401 (2010).
[43] D. Meiser and M. J. Holland, Phys. Rev. A **81**, 033847 (2010).
[44] S. M. Farooqi, D. Tong, S. Krishnan, J. Stanojevic, Y. P. Zhang, J. R. Ensher, A. S. Estrin, C. Boisseau, R. Côté, E. E. Eyler *et al.*, Phys. Rev. Lett. **91**, 183002 (2003).
[45] T. Wang, S. F. Yelin, R. Côté, E. E. Eyler, S. M. Farooqi, P. L. Gould, M. Koštrun, D. Tong, and D. Vrinceanu, Phys. Rev. A **75**, 033802 (2007).

[46] M. Scheibner, T. Schmidt, L. Worschech, A. Forchel, G. Bacher, T. Passow, and D. Hommel, Nat. Phys. **3**, 106 (2007).
[47] R. Raussendorf, D. E. Browne, and H. J. Briegel, Phys. Rev. A **68**, 022312 (2003).
[48] H. Hammer, Opt. Spectrosc. **99**, 320 (2005).
[49] M. Hein, W. Dür, and H.-J. Briegel, Phys. Rev. A **71**, 032350 (2005).
[50] R. I. Karasik, K.-P. Marzlin, B. C. Sanders, and K. B. Whaley, Phys. Rev. A **76**, 012331 (2007).
[51] M. Gross and S. Haroche, Phys. Rep. **93**, 301 (1982).
[52] J. C. MacGillivray and M. S. Feld, Phys. Rev. A **23**, 1334 (1981).
[53] E. Akkermans, A. Gero, and R. Kaiser, Phys. Rev. Lett. **101**, 103602 (2008).
[54] G.-D. Lin and S. F. Yelin, Adv. Atom. Mol. Opt. Phys. **61**, in press (2012).
[55] M. Fleischhauer and S. F. Yelin, Phys. Rev. A **59**, 2427 (1999).
[56] R. Friedberg, S. Hartmann, and J. Manassah, Phys. Rep. **7**, 101 (1973).
[57] J. Deiglmayr, M. Repp, O. Dulieu, R. Wester, and M. Weidemüller, Eur. Phys. J. D **65**, 99 (2011).